

# Implications of Velocity Ratio on the Characteristics of a Circular Synthetic Jet Flush Mounted on a Torpedo Model in Quiescent and Cross-Flow Conditions

A. Kumar<sup>1</sup>, A. K Saha<sup>2</sup>, P. K. Panigrahi<sup>2</sup> and A. Karn<sup>1†</sup>

<sup>1</sup>*Department of Mechanical Engineering, School of Engineering, University of Petroleum and Energy Studies, Energy Acres, Bidholi, Dehradun, Uttarakhand, India 248007*

<sup>2</sup>*Department of Mechanical Engineering, Indian Institute of Technology Kanpur, Kanpur, Uttar Pradesh, India 208016*

†Corresponding Author Email: [akarn@ddn.upes.ac.in](mailto:akarn@ddn.upes.ac.in)

(Received June 29, 2019; accepted November 16, 2019)

## ABSTRACT

A high velocity ratio synthetic jet on an arched surface is of great interest for its potential applications in navy, including torpedo. However, in spite of detailed research on synthetic jets over a flat surface in cross-flow, very few observations have been made on synthetic jets over a surface which is shaped like a torpedo. This study experimentally explores a synthetic jet mounted on a torpedo shaped model in quiescent and cross-flow conditions. Initially, the synthetic jet is characterized for two different diaphragm displacements and at four distinct actuation frequencies in the range of 1 Hz – 6 Hz in a quiescent flow environment. Subsequently, in cross flow, similar study is conducted for three cross-flow velocities ranging from 7.2 – 32 cm/s, at a fixed amplitude of diaphragm oscillations. The measurements are carried out using Laser Induced Fluorescence (LIF) and Laser Doppler Velocimetry (LDV) and the qualitative LIF visualizations are corroborated by the quantitative LDV data. These results indicate that the synthetic jet vortex rings can be grouped as stretched vortex rings and distorted tilted vortex rings. The flow structures primarily depend on the velocity ratio, which is function of cross-flow velocity and frequency of actuation. The flow physics in case of a curved torpedo surface is slightly different as compared to the synthetic jet on a flat surface.

**Keywords:** Synthetic jet; Torpedo model; Vortex rings; Velocity ratio; Jet in cross flow; LIF.

## 1. INTRODUCTION

In the past two decades, synthetic jets have gained considerable attention for a wide array of applications viz. heat transfer enhancement (Chaudhari *et al.* 2010, McGuinn *et al.* 2016), mixing enhancement (Higashiura *et al.* 2007), propulsion & maneuvering (Siekman 1962), drag reduction (Amitay *et al.* 2001) and jet control (Smith and Glezer, 2002). Essentially, a synthetic jet is defined as a train of vortex rings generated by repetitive fluid suction and expulsion through an orifice that does not carry net flux of mass, but still transfers linear momentum to the flow (Kumar and Karn 2018). Figure 1 shows the process of a synthetic jet actuation. As indicated in the figure, actuation system by synthetic jet is usually made of a pendulating diaphragm, a cavity opening and an immovable boundary which encloses to produce a cavity. The diaphragm oscillations are produced at one side of the cavity, and the other side contains an orifice. The fluid suction and fluid discharge rates via

the orifice are regulated by diaphragm oscillations. The vortex ring assisted by its self-effected velocity, moves downstream and interacts with the fluid, it enlarges till a point the energy of the circulation is unable to hold its growing size, eventually leading to its breakup into smaller pieces.

There are many factors that determine the formation and propagation of synthetic jet viz. type of the generation mechanism viz. piston cylinder or oscillating diaphragm method, frequency of jet actuation, volume ejected per cycle, ratio of ejection to suction time, velocity profile of moving piston or diaphragm, orifice shape and thickness, fluid compressibility and the flow environment (Kumar and Karn 2018). Of all these parameters, the effect of the flow configuration is crucial as it has a significant bearing on the resulting vortex dynamics, and it provides a lot of interesting insights into the complex flow physics on the generation and propagation of the synthetic jet.

Usually, in a flow configuration of parallel flow or quiescent flow, simple vortex rings are observed that

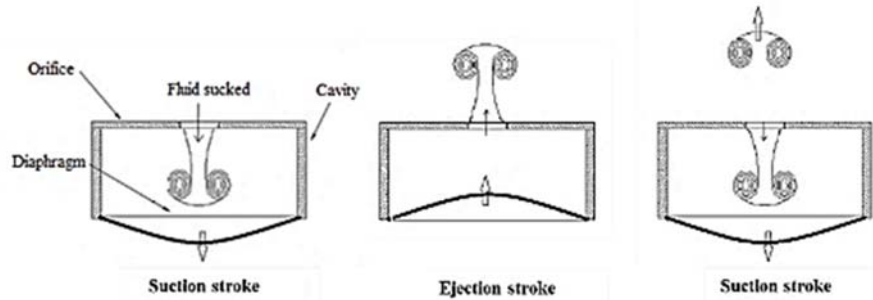


**Fig. 1.** Layout of a synthetic jet actuation using orifice-diaphragm apparatus (Adapted from Kumar and Karn 2018).

depend only on the shape of jet exit. However, additional vortices such as Horseshoe, upright and wall vortices also appear in a jet cross-flow configuration (Kelso *et al.* 1996). In such a cross-flow condition, physics of the flow is determined by the formation of a “train” of distinct vortical structures, that enhances mixing between the flow in the outer layer and the flow in the shear layer close to the wall aiding re-energization of the boundary layer (Prince *et al.* 2012). When a synthetic jet interacts with laminar boundary layer, three types of unique vortical structures hairpin vortices, stretched vortex rings and tilted/distorted vortex rings are reported for synthetic jet in cross-flow (Jabbal and Zhong 2010). In a cross-flow set up, though the generation of these vortex rings may have a dependence upon the velocities of the fluid in perpendicular directions, some past findings have reported that the underlying physics of the flow is determined by the magnitude of ratio of these fluid velocities (referred to as velocity ratio, or  $\bar{v}$ ), more than the rest of the physical variables (Berk *et al.* 2018). As an example, for a circular synthetic jet in cross-flow, actuating between 2Hz to 10Hz in water, it was deduced that the velocity ratio and distance of separation of vortices are primary parameters affecting the synthetic jet in cross-flow (Crook and Wood, 2001). It was reported that the height of jet infiltration and its path is wholly a function of ratio of momentum flux, which is equivalent to velocity ratio (Milanovic and Zaman, 2005).

However, a majority of the prior research on synthetic jets in cross flow has been made on the synthetic jets on a planar surface (for instance, Dai *et al.* 2016, Wen *et al.* 2018). To our best knowledge, very few reports discuss the behavior of a synthetic jet mounted on a curved torpedo-like surface particularly at high velocity ratios, which may be of great interest for its potential utility in naval or other applications. Therefore, in the present paper, we focus our attention on exploring the flow behavior of a circular synthetic jet flush placed on the torpedo-like cylindrical surface in cross flow at various flow conditions vis-à-vis the behavior of a synthetic jet in quiescent flow condition.

## 2. EXPERIMENTAL SETUP AND METHODOLOGY

A model with the shape of a torpedo, with a built-in

synthetic jet production unit is manufactured to study the behavior of synthetic jet in cross-flow environment and is shown in Fig. 2a. The model is 30 mm in radius and is placed within a recirculating horizontal water tunnel. The cross sectional area of square test-section is 160000 mm<sup>2</sup>. The diaphragm is comprised of nylon rubber sheet 1.5 mm thick having an outer and inner diameter of 43.5 mm and 33 mm respectively, with nitrile coating. A leaf spring made from 15 mm wide and 0.5 mm thick carbon steel strip is used to maintain an uninterrupted contact of the cam with the follower, as shown in Fig. 2b. The orifice diameter and thickness are both 6 mm. The laser source is a COHERENT® INNOVA-90, 4W continuous Argon-Ion Laser. A planar and concave cylindrical lens, which has a 15 mm focal length, is used to generate a laser sheet 1.5 mm thick. The LIF images are captured with a resolution of 1280×1280 pixels at a frame rate ranging between 10 and 30 fps using Basler® A501-KC camera. The fluorescein sodium is selected as the dye for LIF imaging. Velocity measurements in the cross streamwise and streamwise direction are carried out using five-beam LDV probe as presented in a recent paper (Kumar and Karn 2018). Silver coated hollow glass spheres in the diameter range of 8 μm -12μm are used for seeding the flow. The velocity data is time-averaged over a duration of 60 seconds, i.e. over 10-60 cycles depending upon the frequency of the synthetic jet. A maximum fluctuation of ± 3.7 % around the mean is observed in the measured velocity components considering uneven sampling. The five-beam probe, mounted on a 2D traverse, moves in transverse plane (YZ-plane) with a resolution of 6.25 μm and an accuracy of ± 300 μm. The cross-flow is obtained by placing the model within water tunnel test section. The actuation frequencies and their corresponding non-dimensional numbers are tabulated in Table 1. It is worth noting that for simplicity, the frequencies are presented in its nearest integer values though the actual values are fractional.

The physical variables considered in the present study are frequency ( $f_{act}$ ) and amplitude ( $\Delta$ ) of oscillation of the actuator, mean jet exit velocity ( $U_{avg}$ ), time of ejection in a cycle ( $T_e$ ), total cycle time ( $T$ ), orifice diameter ( $D$ ) and the geometrical parameters of the diaphragm such as inner cavity diameter ( $D_{ca}$ ) and diameter of the disk ( $D_{cy}$ ). The total cycle time ( $T$ ) is given as the sum of suction and ejection stroke time as  $T = T_s + T_e \approx 2T_e$ , and thus

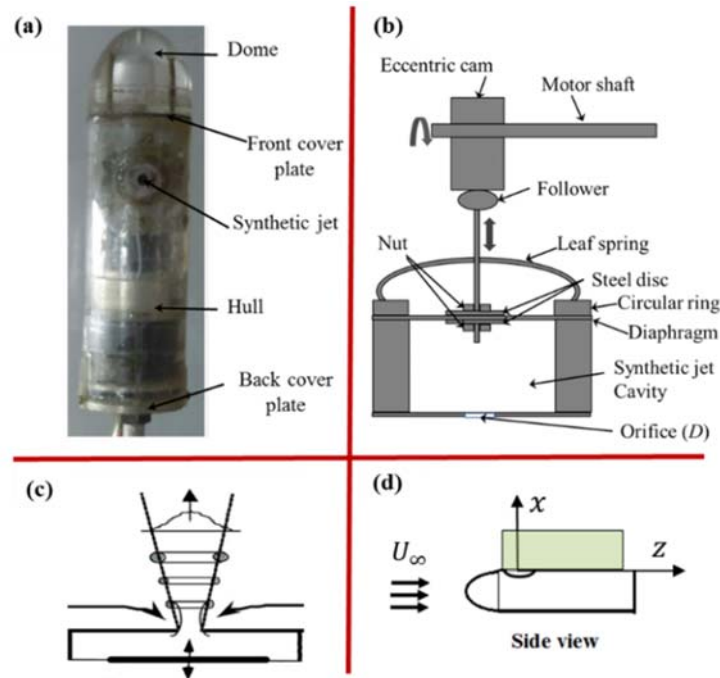


**Fig. 2.** (a) Experimental setup of the synthetic jet embedded in torpedo model, (b) details of actuation mechanism, (c) schematic for cross-section of synthetic jet generation using diaphragm oscillation, and (d) schematic for axis notation and orifice orientation with imaging plane for torpedo model.

**Table 1** Experimental parameters to study the synthetic jet built in on torpedo shape model in quiescent flow

$f_{act}$ (Hz)	$\Delta = 1.5$ mm			$\Delta = 2$ mm		
	$Re$	$St$	$L/D$	$Re$	$St$	$L/D$
1	323	8.5	4.56	425	8.3	6.08
2	550	11	4.56	732	11	6.08
4	1030	15	4.56	1372	15	6.08
6	1544	18.3	4.56	2058	18.3	6.08

the actuation frequency is given by  $f = 1/2T_e$ . As suggested in the prior literature (Mohseni 2006), the ejected volume ( $V_d$ ) for the diaphragm can be computed as  $V_d = \pi\Delta/8(D_{ca}^2 + D_{cy}^2)$ . The mean jet exit velocity and slug length ( $L$ ) can be computed as  $U_{avg} = V_d/A_oT_e$  and  $L = V_d/A_o$ , where  $A_o$  represents the area of cross-section of the orifice. These physical variables can be typically expressed in the terms of dimensionless parameters such as Reynolds number,  $Re = U_{avg}D/\nu$ ; Strouhal number,  $St = f_{act}D/U_{avg}$  and formation number,  $Fn = L/D$ , where  $\nu$  and  $g$  respectively denote the kinematic viscosity of water and acceleration due to gravity. It is also to be noted here that the formation number is simply an inverse of the Strouhal number. The velocity ratio ( $\tilde{v}$ ) is the ratio of the slug velocity ( $U_{avg}$ ) to the cross stream or free velocity ( $U_\infty$ ). Transverse distance and the time are non-dimensionalized with respect to the orifice diameter and the total cycle time and are represented by  $\tilde{x}$  and  $\tilde{t}$ , respectively. The ambiguity in the frequency of actuation of cam actuated synthetic jet is found to be

$\pm 5\%$ . The uncertainty in the Reynolds and Strouhal numbers are equal to  $\pm 5.2\%$  and  $\pm 0.5\%$ , respectively. A  $\pm 8\%$  of uncertainty is obtained in velocity ratio measurement. Based on the area of cross section, the blockage ratio is calculated to be 1.7%, which is within the level of acceptance.

The experimental conditions to analyse the characteristics of synthetic jet in cross-flow are tabulated in Table 2. The position of orifice and the co-ordinate system are also shown in Fig. 2d. In this study, the velocity ratio ( $\tilde{v}$ ) is varied in the range of 0.34 - 4.77, Reynolds number of synthetic jet for no cross-flow condition ( $U_\infty = 0$ ) is fixed at three different values: 732, 1372, and 2058. The actuation frequencies used for synthetic jet in cross flow are 2 Hz, 4Hz and 6 Hz. For cross flow configuration, since no fluid is ejected out of the synthetic jet actuator into the flow regime for the chosen range of cross-stream velocities at a low frequency of 1 Hz, visualization is carried out only in a quiescent environment for the frequency of 1Hz.

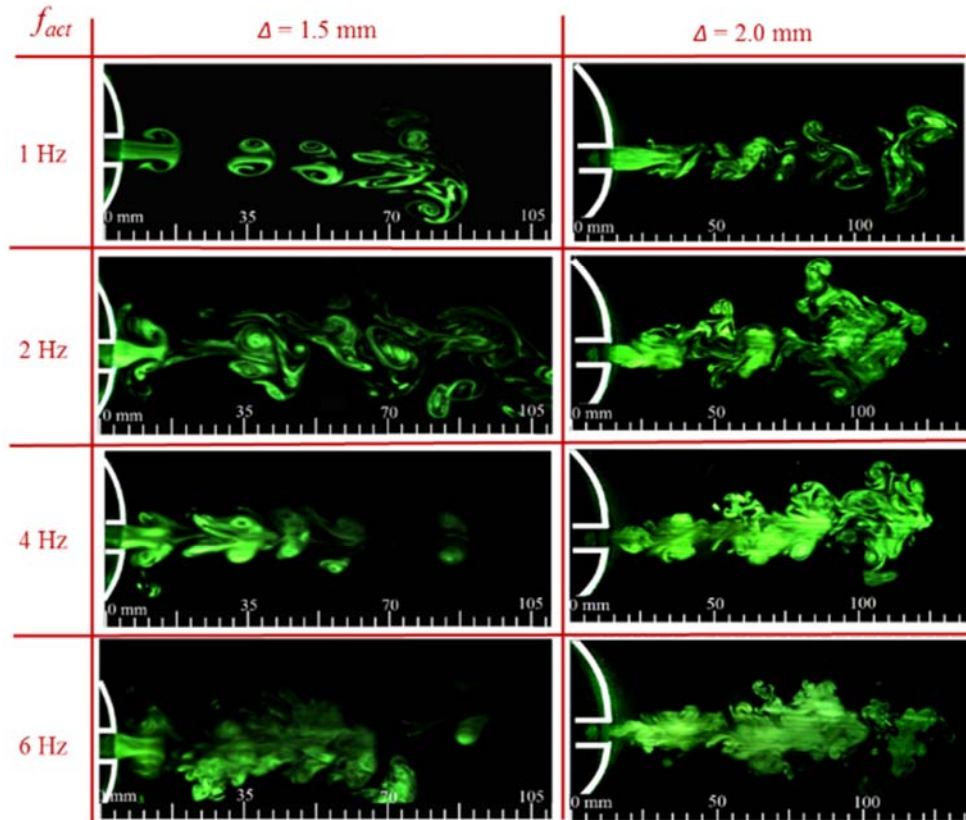


Fig. 3. Sequence of LIF images at  $\tilde{t} \sim 0.75$  in a quiescent flow condition at different frequencies and amplitudes. The shown figures are for time durations covering multiple cycles.

Table 2 Values of the relevant non-dimensional parameters  $Re$  and  $\tilde{\nu}$  with respect to  $U_\infty$  and actuation frequency fact at a fixed  $Fn = 6.1$

$U_\infty$ (cm/s)	$f_{act}$ (Hz)	$Re$	$\tilde{\nu}$
7.2	2	732	1.69
7.2	4	1372	3.18
7.2	6	2058	4.77
20.0	2	732	0.61
20.0	4	1372	1.14
20.0	6	2058	1.72
32.0	2	732	0.34
32.0	4	1372	0.64
32.0	6	2058	0.95

### 3. RESULTS AND DISCUSSION

LIF and LDV measurements are conducted for synthetic jets both in quiescent flow and cross-flow condition at distinct actuation frequencies in the range of 1 Hz – 6 Hz for different amplitude of oscillations for quiescent flow conditions and at a variety of cross-stream velocities for cross-flow conditions.

#### 3.1. Synthetic Jet in Quiescent flow Condition

The flow structures of synthetic jet for two different amplitudes of oscillation and four different frequencies has been illustrated using the visualization images taken on XY-plane bisecting the orifice diametrically have been shown in Fig. 3.

As the figure shows, at a frequency of actuation of 1 Hz, the strength of vortices formed due to the rolling of shear layer coming out of the orifice is found to be weak with low vorticity content. The position of the velocity peak in the jet is governed by Stokes number, which is believed to affect the rolling of shear layer. A lower value of Stokes number (less than 10) restricts shear layer from rolling while a higher value promotes the formation of strong vortex rings (Rathnasingham and Breuer, 1997). An increment in the frequency of actuation raises the amount of fluid expelled out of the orifice, consequently augmenting the jet velocity. This in turn steps up the Stokes number and helps in enhancing the vortex roll up process. Close examination of the images for  $\Delta = 1.5$  mm at different frequencies reveals that the strength of the vortex rings increases while the flow at far downstream becomes complex with increasing small scale structures. The formation of partial trailing jet

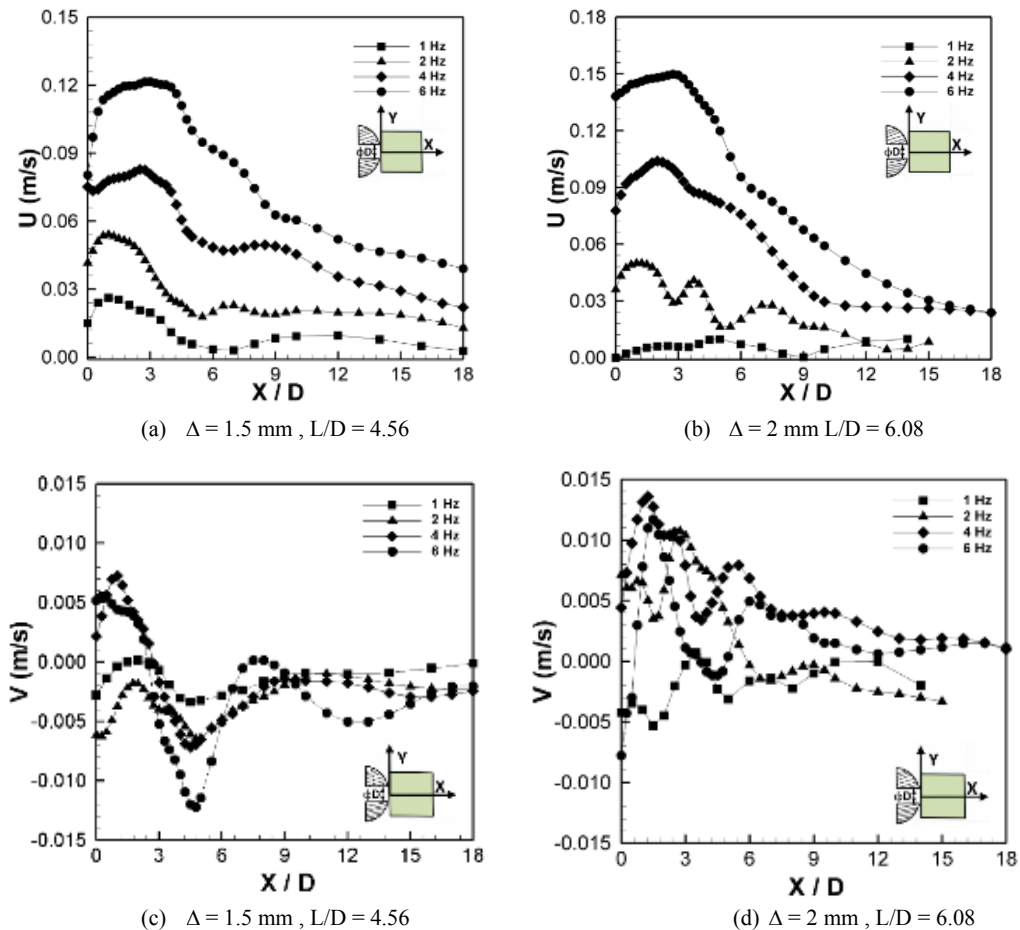


**Fig. 4.** Time averaged streamwise velocity profile (a) and (b) and cross-stream velocity profile (c) and (d) for  $\Delta = 1.5$  mm and  $\Delta = 2$  mm respectively along the synthetic jet centerline.

is also clearly visible for a frequency of actuation 4 Hz. With an increase in  $L/D$  ratio for a diaphragm displacement of  $\Delta = 2$  mm, more elongated and stronger trailing jet has been observed to form as compared to a smaller diaphragm displacement of  $\Delta = 1.5$  mm. As frequency increases, increasingly stronger and longer trailing jet is seen for  $\Delta = 2$  mm as demonstrated in Fig. 3.

In the LIF experiments, the dye is injected once into the cavity before the images are captured. Sometimes, the leftover dye from the last cycle also gets illuminated along with the ejected fluid, giving an appearance of existing fluid velocity in the regions where there is not much velocity. Conversely, if the dye intensity is less in some region, although it may not be captured in the LIF visualization, yet, the velocity field will be measured accurately using LDV. Thus, due to dye attenuation, minor discrepancies between LIF and LDV are expected. Some differences between the LIF measurements and the LDV measurements are also obvious since the former is instantaneous while the latter entails time-averaging. Thus, since all the LIF images shown are instantaneous snapshots and there are many random effects that disturb the jet flow,

these images cannot qualitatively characterize and completely capture the mechanism behind jet curvature. As mentioned before, once the synthetic jet is actuated, the LIF images are captured after few cycles, and it is indeed possible that such different trajectories may only happen during the initial stages of the synthetic jet actuation. Therefore, to gain a better insight into the flow physics, the time averaged LDV measurements are also discussed below.

The two different velocity components namely, streamwise velocity (in the direction of synthetic jet) and the cross-stream velocity have been measured using LDV for two amplitudes and four different actuation frequencies. The axial variation of the two components of velocity is shown along the centerline of synthetic jet in Fig. 4. For both amplitudes, the streamwise velocity is observed to have a monotonic behaviour with the axial distance. As expected, the time-mean velocity in the near vicinity of orifice increases with increasing frequency. The velocity remains higher and almost at constant value until  $X/D \sim 4$ , followed by a rapid fall up to  $X/D \sim 9$ , and then decreases slowly with axial distance. This trend matches with the normal trend of velocity variation observed for synthetic jet in quiescent flow where the

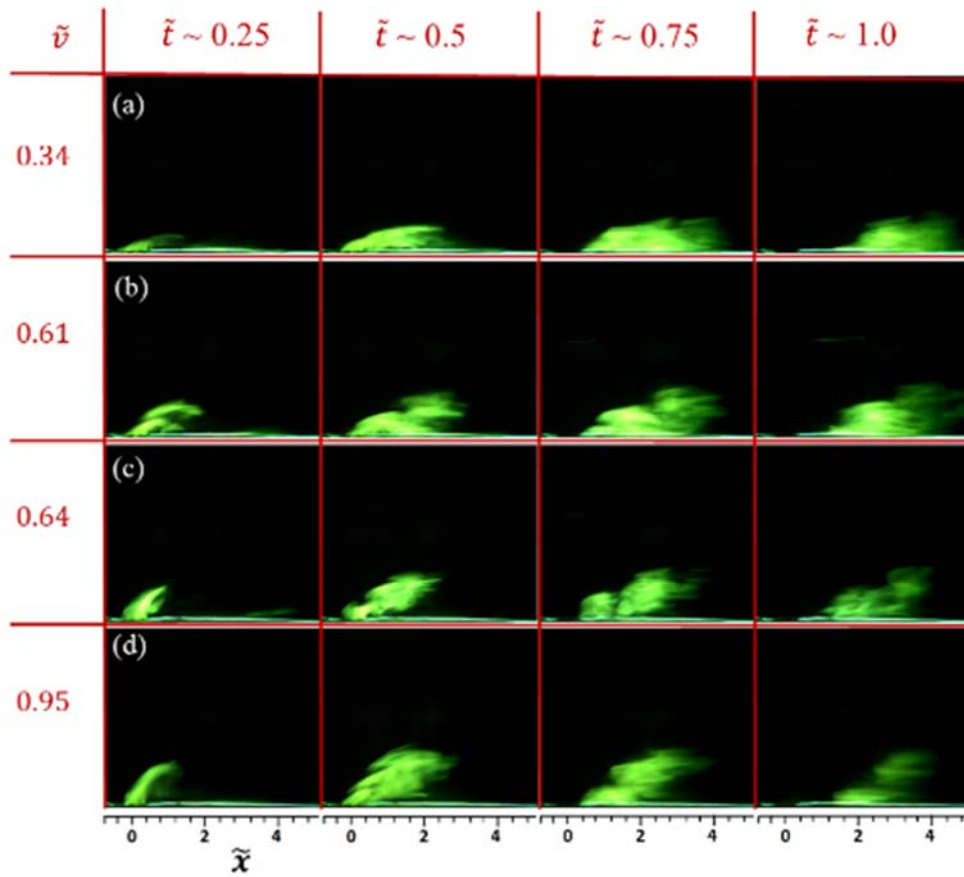


Fig. 5. It can be suggested that the curved surface would have a more prominent effect on the synthetic jet at low velocity ratios owing to the boundary layer pressure gradient in which the synthetic jet is embedded. LIF images taken in a cross-flow condition for low velocity ratios at different time stamps for (a)  $f_{act} = 2$  Hz,  $U_{\infty} = 32$  cm/s; (b)  $f_{act} = 2$  Hz,  $U_{\infty} = 20$  cm/s ; (c)  $f_{act} = 4$  Hz,  $U_{\infty} = 32$  cm/s and (d)  $f_{act} = 6$  Hz,  $U_{\infty} = 32$  cm/s.  $\tilde{t}$  denotes the non-dimensional time, or time scaled with respect to the cycle time of oscillation,  $T$ . The scale bar of  $\tilde{x}$  at the bottom denotes distance in the transverse direction, non-dimensionalized with respect to orifice diameter,  $D$ .

jet producing device is attached to one of its wall. The undulation of the streamwise velocity in the near field in Fig. 4(b) at 2 Hz may be attributed to the leap forging motion of vortex rings as observed in the sequence of LIF images in Fig. 3. The positive value of cross-stream velocity component ( $V$ ) represents the fluid flow outwards from the jet centerline while negative value signifies the flow towards the centreline. The vortex rings at  $\Delta = 1.5$  mm are found to be quite coherent with weak trailing jet. The coherent nature of the ring leads to monotonic distribution of cross-stream velocity shown in Fig. 4 (c). But a non-monotonic distribution in Fig. 4 (d) for  $\Delta = 2$  mm may be due to chaotic or probably turbulent nature of jet that has small scale structures in trailing jet as noticed in Fig. 3.

### 3.2. Synthetic Jet in Cross-Flow Condition

As discussed in the previous section, it has been observed that higher diaphragm displacement contributes to a stronger trailing jet. The secondary vortices or trailing jet of synthetic jet in cross-flow induces streamwise tertiary vortices near the wall. In

a time-averaged sense, these vortices corresponding to the legs embedded in a boundary layer have characteristics similar to a pair of longitudinal vortex giving a common downwash. Since the higher diaphragm displacement yields a complicated flow physics, an optimal diaphragm displacement of  $\Delta = 2$  mm is chosen for the study of synthetic jet in cross-flow.

Flow structures' analysis of visualization images at various frequencies and cross-flow velocities shows that the flow structures and formation of synthetic jet seem to definitely indicate a dependence upon frequency of actuation and cross-flow velocity. However, a systematic examination of the visualization of flow patterns reveals that rather than the frequency of actuation or the cross-flow velocity,  $\tilde{v}$  is the single most important parameter that characterizes a jet in a cross-flow configuration. Therefore, the LIF flow visualizations on XZ-plane are conducted, aimed at comparing the flow structure of synthetic jets upon variation in  $\tilde{v}$ .

Figure 5a shows that at the lowest  $\tilde{v}$  (0.34 at 2 Hz),

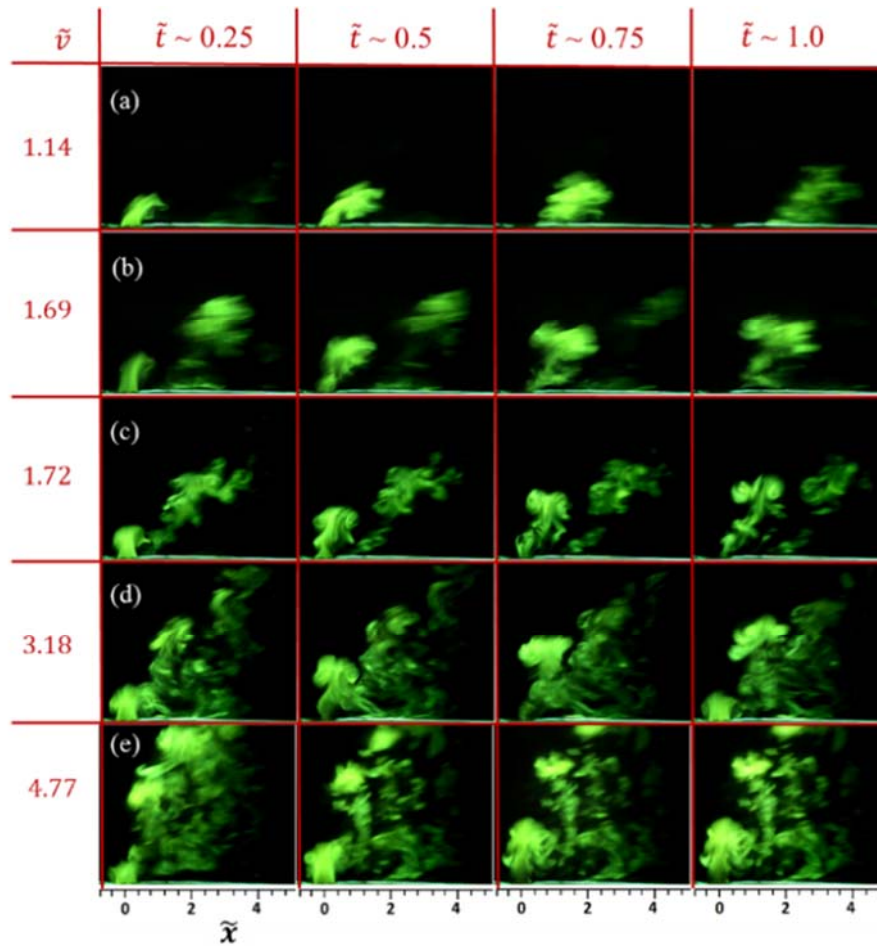


**Fig. 6.** LIF images taken in a cross-flow condition for high velocity ratios at different time stamps for (a)  $f_{\text{act}} = 4$  Hz,  $U_{\infty} = 20$  cm/s; (b)  $f_{\text{act}} = 6$  Hz,  $U_{\infty} = 20$  cm/s; (c)  $f_{\text{act}} = 2$  Hz,  $U_{\infty} = 7.2$  cm/s; (d)  $f_{\text{act}} = 4$  Hz,  $U_{\infty} = 7.2$  cm/s and (e)  $f_{\text{act}} = 6$  Hz,  $U_{\infty} = 7.2$  cm/s.  $\tilde{t}$  denotes the non-dimensional time, or time scaled with respect to the cycle time of oscillation,  $T$ . The scale bar of  $\tilde{x}$  at the bottom denotes distance in the transverse direction, non-dimensionalized with respect to orifice diameter,  $D$ .

the hairpin vortices are formed. Asymmetric vortex rings are typically produced when the synthetic jet experiences a cross-flow. Since  $\tilde{v}$  is quite low, the upstream part of the vortex ring is weak and gets stretched significantly and envelops the downstream part of the vortex. It is also expected that the jet formed in quiescent flow is quite elongated because of the formation of trailing jet at higher  $L/D$  ratio. Under the action of the cross-flow, more stretching of the vortex structure cause it to transform into a stretched vortex ring at  $\tilde{t} = 1$ . Since the imaging plane bisects the hairpin vortices and shows only a slice in XZ-plane, both the legs of stretched vortices are not visible. Therefore, only the leading vortex along with thin shear layer upstream is captured by LIF technique. A higher value of stroke length ( $L/D = 6.08$ ) and a lower value of  $\tilde{v}$  (0.34) keep the vortices attached to the wall and the non-linear interactions between the boundary layer and the stretched vortices cause the structures to break after traveling a considerable distance downstream. Similar trend in vortex dynamics in case of stretched

vortex ring at  $L/D = 6.67$  for a circular orifice has also been reported by [Chaudhry and Zhong \(2014\)](#). It has been observed that at low  $\tilde{v}$ , the synthetic jet remains within the boundary layer. Therefore, it has been suggested that synthetic jet at low  $\tilde{v}$  may prove to be effective in controlling the boundary layer ([Jabbal and Zhong 2008](#)). As illustrated in Fig. 5b, the difference in the structures between  $\tilde{v} = 0.61$  and  $\tilde{v} = 0.34$  exists only in the near orifice field. The upstream part of vortex ring being weaker is swept away faster than the downstream part of the ring and rides over the downstream part. While traveling downstream, they also get stretched but remain close to the wall. As evident from Fig. 6a, the flow structures change significantly upon a slight increment in  $\tilde{v}$  (0.64, 0.95 and 1.14). The vortex rings are observed to penetrate more compared to  $\tilde{v} = 0.34$  and 0.61 in the vertical direction before being convected in the cross-flow direction. Unlike low  $\tilde{v}$  cases ( $\tilde{v} = 0.34$  and 0.61), the jet does not bend much but stretching of the jet is quite distinct. The trailing jet behind the tilted and distorted leading vortex ring

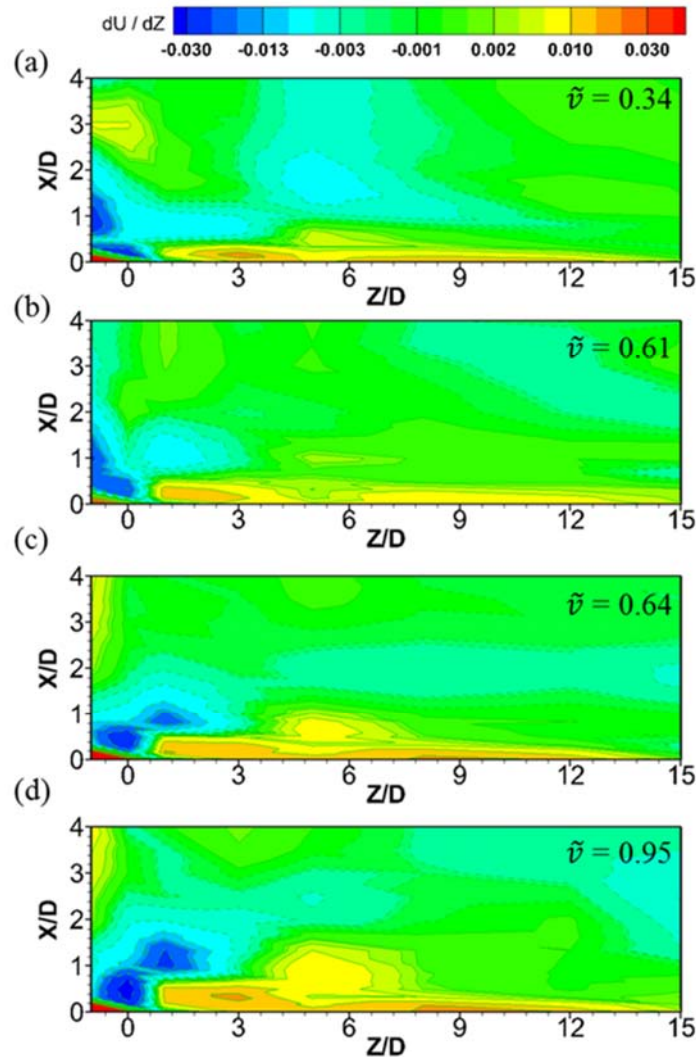


**Fig. 7. Contour plots of the velocity magnitude measured using LDV for low velocity ratios at different time stamps for (a)  $f_{act} = 2$  Hz,  $U_{\infty} = 32$  cm/s; (b)  $f_{act} = 2$  Hz,  $U_{\infty} = 20$  cm/s ; (c)  $f_{act} = 4$  Hz,  $U_{\infty} = 32$  cm/s and (d)  $f_{act} = 6$  Hz,  $U_{\infty} = 32$  cm/s. The origin in these contour plots coincides with the orifice centre. The dotted lines and the solid lines denote the negative and positive velocity gradient regions, respectively.**

without any distinct breakages are observed for  $\tilde{v} = 0.64$  to 1.14. In this range of  $\tilde{v}$ , jet has low Reynolds number but still a high Stroke length. Also a strong trailing jet follows the leading vortex ring for a longer duration.

When the values of  $\tilde{v}$  are further increased, the flow structure gets significantly altered, as shown in Fig. 6b for  $\tilde{v} = 1.69$ . Due to higher momentum of synthetic jet in comparison to cross-flow, the leading vortex ring penetrates much well above the boundary layer and travel downstream. The trailing jet being weaker diffuses very quickly. When  $\tilde{v}$  is increased further (1.72, 3.18 and 4.77), the jet penetrates deep into the core of the cross-flow without bending much in the flow direction (Fig. 6c-6e). The tilted vortex rings experience no substantial stretching or distortion. The formation of long trailing jet or secondary vortices with multiple scales at  $\tilde{v} = 3.18$

and 4.77 confirms the incoherent nature of the trailing jet. For this higher  $\tilde{v}$ , the leading vortex ring having higher self-induced velocity follows a trajectory different from the trailing jet covering the entire span between the trajectory of leading vortices and the wall. As a result of high values of induced velocity and momentum, the leading vortex ring detaches itself from wall and moves into the core cross-flow. In case of deformation of trailing jet in the form of hairpin structure behind the tilted vortex ring it is observed to shed itself coherently as shown in Fig. 5.

Figures 7 and 8 present the contour plots of the velocity gradient in the cross-streamwise direction ( $dU/dZ$ ), measured using LDV in the  $xz$ -plane passing through the orifice centre across a range of velocity ratios ( $\tilde{v} = 0.34 - 4.77$ ). It should be pointed out that the LDV measurement plane is identically

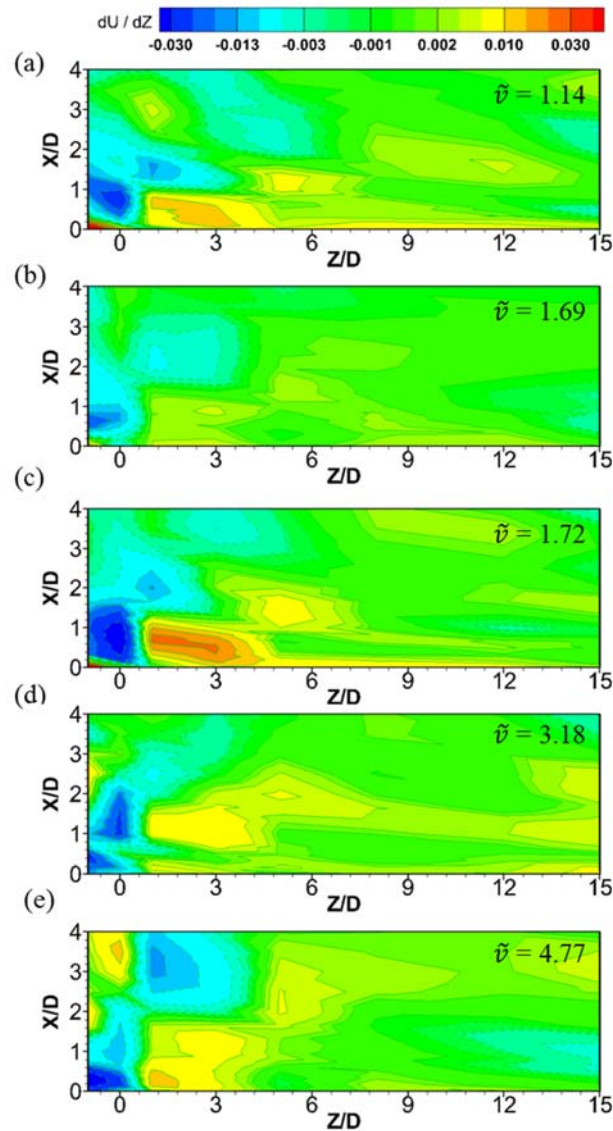


**Fig. 8. Contour plot of velocity magnitude measured using LDV in the cross-flow condition for high velocity ratios at different time stamps for (a)  $f_{act} = 4$  Hz,  $U_{\infty} = 20$  cm/s; (b)  $f_{act} = 6$  Hz,  $U_{\infty} = 20$  cm/s; (c)  $f_{act} = 2$  Hz,  $U_{\infty} = 7.2$  cm/s; (d)  $f_{act} = 4$  Hz,  $U_{\infty} = 7.2$  cm/s and (e)  $f_{act} = 6$  Hz,  $U_{\infty} = 7.2$  cm/s. The origin in these contour plots coincides with the orifice centre. The dotted lines and the solid lines denote the negative and positive velocity gradient regions, respectively.**

the same as the plane of imaging in the LIF visualization, although as discussed before, some minor differences between the observations of the flow structures obtained from LIF and LDV are expected. It is interesting to note that these contour plots depict the distribution of velocity gradient and not the velocity magnitudes, and it is preferable to draw the distribution of velocity gradient because it provides an insight into the shear stress or the stretching of vortex structures in the flow field. In these contour plots, two distinct flow regimes can be observed: one with a positive cross-stream velocity gradient, and the other with a negative cross-stream velocity gradient. As the synthetic jet emerges from

the orifice, a pair of counter-rotating vortices forms due to shear layer roll-up, as can be observed in the  $xz$ - plane. However, due to the presence of the cross-flow, the vortex on the upstream side opposes the cross-stream velocity whereas the downstream side is assisted by the presence of the cross-flow. This superposition of velocities leads to the weakening of the vortex in the upstream side, whereas the other downstream part of the vortex gets strengthened, leading to the existence of two disparate velocity gradient regions. As shown in Fig. 7a, when  $\tilde{v}$  is very low ( $\tilde{v} = 0.34$ ), the synthetic jet does not protrude into the flow, and consequently it becomes greatly stretched leading to interconnected

and tightly spaced hairpin vortices at a downstream location that remain close to the wall, possibly within the boundary layer. When the cross-flow velocity is slightly reduced or the actuation frequency is increased, leading to a greater  $\bar{v}$  (such as  $\bar{v} = 0.61, 0.64$ ), the synthetic jet can be seen to protrude more into the flow, although there is significant stretching of the downstream portion of the synthetic jet. As presented in Fig. 7b and 7c, this stretching is extended further away of the wall, as compared to the previous case. Figure 7d illustrates the effect of increasing  $\bar{v}$  to 0.95, and the presence of the two distinct positive and negative velocity gradient regions are markedly observed, which match closely with the LIF visualization. In this case, the jet does not bend although the stretching of the jet is quite distinct. The trailing jet behind the tilted and distorted leading vortex ring without any distinct breakages can also be observed. Further, as  $\bar{v}$  is subsequently increased from 1.14 to 4.77, as displayed in Fig. 8, a striking observation can be made: Not only the respective values of velocity gradients increase in the counter-rotating vortex pair, but also owing to greater momentum of synthetic jet in comparison to cross-flow, the leading vortex ring penetrates much more above the boundary layer and travels downstream, whereas the trailing jet undergoes diffusion being much weaker in intensity. When the  $\bar{v}$  is increased further to larger values (1.72, 3.18 and 4.77), the synthetic jet penetrates deep into the core of the cross-flow without undergoing much bending in the cross-streamwise direction, as shown in Figs. 8b to 8e. The tilted vortex rings experience no substantial stretching or distortion, and the trailing jet is non-coherent. As a final point, it should also be pointed out that the existence of these positive and negative velocity gradient regions, as shown by these contour plots evidently ascertain the differences in flow field as compared to a synthetic jet mounted on a flat surface. Thus, the LIF and LDV measurements corroborate each other and suggests that the flow physics and its unsteady behavior depend primarily upon the velocity ratio, particularly for jet in a cross flow. At a low velocity ratio, it is mainly the hairpin vortices that behave akin to the counter-rotating vortex pair that dominate the jet in cross-flow. As the velocity ratio increases, the conventional jet in cross-flow topology recovers and counter-rotating vortex pair becomes the characteristic feature of the jet in cross-flow and it persists farther downstream.

#### 4. CONCLUSIONS

In a quiescent flow condition, it was observed that at a low frequency of 1 Hz, the strength of vortices due to rolling of shear layer is weak with low vorticity content. Increase in the jet velocity is brought about by an increase in the frequency of actuation, and initially enhances the vortex roll up process and later leads to the formation of more small scale structures. Raising the amplitude of the diaphragm oscillations generates increasingly stronger and longer trailing jets. For the cross-flow conditions, the behaviour of synthetic jet is investigated at three different actuation frequencies with velocity ratios varying

between 1.69 and 4.77. Our experiments have demonstrated that velocity ratio is an important parameter that characterizes a jet in cross-flow. Stretched and elongated leading vortex ring, which occurs at low  $\bar{v}$  and remains attached to wall results in the formation of a hairpin structure or transformed into a stretched vortex ring. Since at low  $\bar{v}$  (0.34 to 0.6) the maximum portion of hairpin legs are near the wall, these may create a downwash bringing fluid with large momentum towards the wall from core flow and hence, cause an upsurge in the local shear stress. On the other hand, at moderate  $\bar{v}$  (0.6 to 1.2), a transition is observed where the vortex stretching is minimum and only the trailing end of synthetic jet is connected to the wall. Finally, at very high values of  $\bar{v}$ , the vortex rings get completely detached from the wall and flow with the free stream. Initially, it was expected that the curved surface area of the synthetic jet would allow for greater fluid entrainment from the sides during the suction stroke. The curvature effect clearly gets manifested by the existence of the positive and negative velocity gradient regions near to the wall, which is clearly distinct as compared to a synthetic jet mounted on a flat surface. A greater effect due to the curvature can be observed at lower jet-to-free stream velocity ratios, which leads to a slower penetration of the synthetic jet out of the boundary layer. Using a circular synthetic jet in both quiescent and cross-flow, actuating between 1Hz to 6Hz in water, and spanning across a wide range of velocity ratios, it was deduced that the velocity ratio is a primary parameter affecting the synthetic jet in cross-flow. The current work may prove beneficial for the validation of computational simulations conducted on a curved torpedo surface for naval or other applications.

#### REFERENCES

- Amitay, M., D.R. Smith, V. Kibens, D.E. Parekh and A. Glezer (2001). Modification of the Aerodynamics Characteristics of an Unconventional Airfoil Using Synthetic Jet Actuators. *AIAA Journal* 39(3), pp. 361- 370.
- Berk, T., N. Hutchins, I. Marusic, and B. Ganapathisubramani (2018). Trajectory of a synthetic jet issuing into high-Reynolds-number turbulent boundary layers. *Journal of Fluid Mechanics* 856, 531-551.
- Chaudhari, M., B. Puranik and A. Agrawal (2010). Effect of orifice shape in synthetic jet based impingement cooling. *Experimental Thermal and Fluid Science* 34, 246-256.
- Chaudhry, I. A., and S. Zhong (2014). A single circular synthetic jet issued into turbulent boundary layer. *Journal of Visualization* 17(2), 101-111.
- Crook, A., and N. Wood (2001). *Measurement and visualisations of synthetic jets*. Nevada, s.n.
- Dai, C., L. Jia, J. Zhang, Z. Shu and J. Mi (2016). On the flow structure of an inclined jet in crossflow at low velocity ratios. *International Journal of*

- Heat and Fluid Flow* 58, 11-18.
- Higashiura, M., K. Inose, M. Motosuke, and S. Honami (2007). *The Effects of the Synthetic Jet on the Mixing Promotion in Low Reynolds Number*. In ASME/JSME 2007 5th Joint Fluids Engineering Conference (pp. 1503-1511). American Society of Mechanical Engineers.
- Jabbal, M., and S. Zhong (2008). The near wall effect of synthetic jets in a boundary layer. *International Journal of Heat and Fluid Flow* 29,119-130.
- Jabbal, M., and S. Zhong (2010). Particle image velocimetry measurements of the interaction of synthetic jets with a zero-pressure gradient laminar boundary layer. *Physics of Fluids* 22, 1-17.
- Kelso, R. M., T. T Lim and Perry (1996). An experimental study of round jets in cross-flow. *Journal of Fluid Mechanics* 306, 111-144.
- Kumar, A., and A.Karn (2018). Qualitative and quantitative characterization of a synthetic jet mounted on a convex torpedo-like surface under cross-flow. *International Journal of Heat and Fluid Flow* 74, 198-208.
- McGuinn, A., D. I. Rylatt and T. S O'Donovan, (2016). Heat transfer enhancement to an array of synthetic air jets by an induced crossflow. *Applied Thermal Engineering* 103, 996-1003.
- Milanovic, I., and Zaman, K (2005). Synthetic jet in cross flow. *AIAA* 43(5), 929-940.
- Mohseni, K (2006). Pulsatile vortex generators for low- speed maneuvering of small underwater vehicles. *Ocean Engineering* 33,2209-2223.
- Prince, S. A., V. Khodagolian and R. Gaid (2012). An experimental study of a pulsed air jet and an acoustic jet on a low speed turbulent boundary layer. Brisbane, AU, *28th International congress of the Aeronautical sciences*.
- Rathnasingham, R. and T. S Breuer (1997). Coupled fluid- structural characteristics of actuators for flow control. *AIAA* 35(5), 832-837.
- Siekmann, J (1962). On a pulsating Jet from the end of a tube, with application to the propulsion of certain aquatic animals. *Journal of Fluid Mechanics*, 15(3), 3
- Smith, B. L., and A. Glezer (2002). Jet vectoring using synthetic jets. *Journal of Fluid Mechanics* 458, 1-34.
- Wen, X., Y. Liu., and H. Tang (2018). Near-field interaction of an inclined jet with a crossflow: LIF visualization and TR-PIV measurement. *Journal of Visualization* 21(1), 19-38.